

Active Semantic Perception

Huayi Tang and Pratik Chaudhari

Abstract—We develop an approach for active semantic perception which refers to using the semantics of the scene for tasks such as exploration. We build a compact, hierarchical multi-layer scene graph that can represent large, complex indoor environments at various levels of abstraction, e.g., nodes corresponding to rooms, objects, walls, windows etc. as well as fine-grained details of their geometry. We develop a procedure based on large language models (LLMs) to sample plausible scene graphs of unobserved regions that are consistent with partial observations of the scene. These samples are used to compute an information gain of a potential waypoint for sophisticated spatial reasoning, e.g., the two doors in the living room can lead to either a kitchen or a bedroom. We evaluate this approach in complex, realistic 3D indoor environments in simulation. We show using qualitative and quantitative experiments that our approach can pin down the semantics of the environment quicker and more accurately than baseline approaches. The source code and additional information can be found on https://github.com/grasp-lyrl/active_semantic_perception.

syntax: the way in which linguistic elements are put together to form constituents such as phrases or clauses;
semantics: dealing with the relations between signs and what they refer to.

I. INTRODUCTION

Suppose you are trying to quickly find milk in a new convenience store. Completing this task requires observing the structure of the environment, e.g., where aisles are located, what objects they contain, etc. It also requires some guesswork as to where the cold storage could be (usually at the back of the store). Finally, it requires the knowledge that if there is no cold storage in sight, it is sensible to give up on finding milk altogether. Plenty of tasks have this flavor, from mundane ones such as finding milk, to critical ones such as a firefighter rescuing a person from a building. Humans are spectacular at these tasks. Robots cannot perform these kinds of tasks. This is not due to the lack of the ability to sense or to move. Robot sensing and mobility are extremely good today—if not as good as that of humans yet.

Perhaps the key distinguishing factor is that humans and robots build very different representations. While robots represent their environment in highly detailed ways in terms of its geometric or photometric properties, human representations are much richer in their semantics. This is why, in spite of often having much poorer fine-grained representations—most of us would be hard-pressed to remember the size of our living room—humans can perform these canonical search tasks much better. This is perhaps how humans can perform “guesswork” and use “knowledge” in the example above.

How should robots build semantic representations of their environment? The Merriam-Webster dictionary defines:

Therefore, the structure of the scene, its geometric and photometric properties as well as the identities of objects in the scene are syntactical entities. Semantics refers to the relationships between these entities. The fact that we find a convenience store without cold storage unusual, although such a store would be perfectly valid, is about us attributing meaning to a collection of objects (and finding it inadequate) [1–3]. **Active semantic perception refers to building a representation of the scene, say our convenience store, and using the semantics of the scene to perform the task, such as finding milk quickly.**

Active perception [5] requires a robot to (a) maintain a representation of the scene that summarizes past observations and update it to incorporate new observations (a map), (b) synthesize new observations of the scene (a generative model), and (c) to select controls that maximize an information gain (planning) [6]. These three tenets motivate our approach described in Fig. 1. First, we argue that a scene graph, e.g., [4, 7], is well-suited for active semantic perception. We build a compact, hierarchical multi-layer scene graph that captures rooms, objects, negative space, and structural boundaries such as walls, doors, and windows. We show that it can represent large, complex environments at various levels of abstraction, e.g., objects inside a room and rooms within a house. The hierarchy enables richer semantics that allows complex inferences for active perception. At the same time, a scene graph can also represent fine-grained details of the geometry and photometry for navigation. Second, we develop a procedure based on large language models (LLMs) to synthesize a new plausible scene graph of unobserved regions that is consistent with partial observations of a scene graph and contains semantically interesting regions, e.g., synthesizing a bedroom and a kitchen after observing the living room. These scene graphs are often metric-accurate, e.g., the coffee table is towards the center of the living room. This generative model allows us to compute an information gain of a potential waypoint which reflects the reduction in the semantic uncertainty of the scene graph for sophisticated spatial reasoning, e.g., the two doors in the living room can lead to either a kitchen or a bedroom. Third, we use a hierarchical planning framework to compute high-level waypoints on the scene graph that correspond to low-level collision-free trajectories that can be executed by the robot.

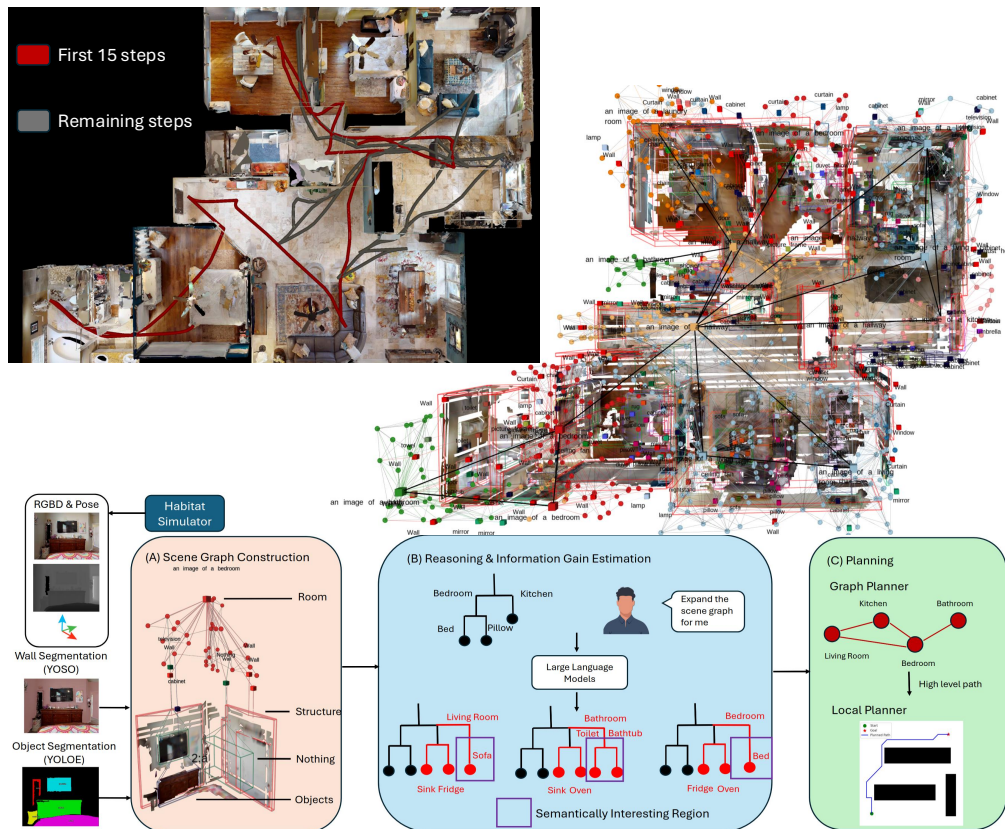


Fig. 1: Top (left): A robot exploring an indoor environment using our proposed method. The first 15 exploration steps are highlighted in red, while the remaining steps shown in gray. The robot quickly covers most semantically salient regions in spite of visual occlusions and narrow corridors/doors, after which it explores the semantic details of the scene. **Top (right):** The final scene graph and mesh constructed after the robot fully explores the environment (visualization using Clío [4]). **Bottom:** Our approach consists of three main components. The scene graph construction/mapping module (A) takes RGB-D and pose from Habitat simulator, object segmentation from YoloE, wall segmentation from YOSO as input, and constructs a multi-layer scene graph with four elements: rooms, structures, “nothing” and objects. The reasoning and information gain estimation module (B) provides the scene graph and a user prompt as input to an LLM, to generate putative scene graphs that are consistent with the current scene graph. The panel shows three such samples, with the most informative region highlighted by the purple rectangle. The planning module (C) includes a graph planner that computes a high-level path over the scene graph, which is executed by an occupancy grid-based local planner.

We evaluate our approach in simulation, in multiple complex 3D indoor environments, and show that it can recover scene semantics faster and more accurately than baseline methods. While hypothesized scene graphs need not necessarily match the true environment, our approach generates plausible predictions that, when aligned with the true scene, enable more efficient retrieval tasks. Our approach can run on a standard GPU-enabled laptop.

II. RELATED WORK

Map Representations Classical volumetric approaches discretize space and store either occupancy probabilities [8] or signed distance functions [9]. While effective for representing geometry, such maps are largely semantics-agnostic. Recent work augments volumetric maps with per-voxel/per-region annotations of the categories of the corresponding objects [10]. Even with an octree-based implementation, this representation remains dense and low-level, making high-level reasoning costly and impractical. A large body of work on neural representations has also emerged recently. Neural radiance fields (NeRF) [11] and 3D Gaussian Splatting [12] are

photorealistic scene representations, and recent extensions incorporate semantics into these models [13, 14]. These methods are however designed for rendering rather than for representing semantics. Extracting explicit geometry of the scene requires dense sampling (e.g., ray marching), which is computationally demanding, and even when accelerated by Gaussian splatting, the result is still a dense, unstructured representation. Such representations do not expose discrete objects or spatial relations, making it difficult to support predictive reasoning about unobserved regions. In this work, we intend to use scene graph to record all geometric and semantic information and form a sparse and hierarchical abstraction of the scene. This makes inference about both observed and unobserved parts of the environment easier.

Exploration methods can be categorized into frontier-based and information-driven approaches. Frontier-based strategies navigate toward the boundary between free and unknown regions [15, 16], while information-driven approaches evaluate candidate viewpoints or trajectories using measures of expected information gain [6, 17–20]. Hybrid

methods combine these ideas by prioritizing frontiers according to their expected informativeness. These methods succeed at identifying unexplored areas but not necessarily on semantically interesting regions. The reason is twofold: first, many representations—such as occupancy grids—only encode geometry. Second, even when some notion of semantics is included, existing methods lack a mechanism for reasoning about unexplored areas, i.e., predicting what is likely beyond currently observed regions. As a result, they may prioritize geometrically novel but semantically unhelpful areas. Dense maps such as occupancy grids further complicate reasoning due to their size and low-level nature.

Recent works have explored integrating semantics into object-goal navigation. SemExp [21] trains high-level policies to predict long-term goals that are semantically correlated with a user-specified task, with a local planner executing the navigation. StructNav [22] instead leverages large language models to rank geometric frontiers according to task relevance, and then passes execution to a local planner. While both approaches incorporate semantics and perform well at locating predefined object categories, they remain tied to fixed vocabularies and do not generalize to reasoning about semantically uncertain regions.

III. METHODS

Our framework comprises of a mapping module, a reasoning module and a planning module, as shown in Fig. 1. The mapping module takes in RGB-D, segmentation images, localization poses, and outputs an ensemble of scene graphs. The reasoning and information gain estimation modules take in these scene graphs, samples semantically consistent potential completions and identifies the region with the highest information gain. This is then passed to the planning module to generate collision-free path for the robot to follow.

A. Mapping

Our approach for building the scene graph, denoted by G , builds upon Clio [4] and contains four types of nodes.

Object nodes: To ensure both speed and accuracy of detection, we choose a unified and single stage architecture, YOLOE [23], instead of FastSAM[24] and CLIP[25] based approach used in Clio. In our experience, this gives a better recall which is important for active perception. We construct a 3D voxel map (based on the depth of the pixels) for every segmentation. We also maintain a set of active tracks to track and estimate objects. Under the assumption that objects cannot move far away between two observations, we can greedily associate new observations to the best fitting track by computing the IoU of the voxel in the current observation and voxel stored in the track. We also require the label to be the same for a successful association. If we cannot associate the new observation with any track, we create a new track for it. Finally, if a track has not been associated for τ seconds, it is terminated. We then reconstruct the object for every track by performing marching cubes [26] algorithm and fit a bounding box to the meshes. This ensures that the bounding box fits the object tightly.

Room nodes: Just like Clio, we construct a truncated SDF for the background and integrate it into an Euclidean

SDF using brushfire algorithm [9]. We extract the sub-graph of places using a Generalized Voronoi Diagram built on the fly while computing the ESDF. For each “place” node, we compute a feature vector by encoding images in which the node is visible using CLIP and averaging the resultant embeddings. We add occlusion checking to the original Clio implementation to make these features more accurate. Next, we apply agglomerative clustering to group multiple “place” nodes into higher-level “room” nodes. The feature of a “room” is defined as the average embedding of its constituent “place” nodes, and its position is set to their mean spatial coordinate. Finally, we assign a “room” label by matching the aggregated feature to the closest predefined “room” category.

“Nothing” nodes: A scene graph is inherently sparse, and constructing a realistic and informative representation of the environment for our tasks requires more than simply modeling objects and rooms. Absence is also informative: RGB-D images and segmentation results not only reveal where objects are present, but also where no objects exist in the scene. We encode this negative space by introducing a nothing object, which explicitly represents regions confirmed to be free of objects. For the current active TSDF map, we threshold it to form the 3D occupancy grid and then identify the largest cuboid in free space within it. This is achieved by extending the classic problem of finding the largest rectangle in a histogram into three dimensions. Because the TSDF map is confined to a local area and efficient algorithms exist for the 2D formulation, this extension remains computationally lightweight.

Structure nodes: In the scene graph, “room” nodes only store positional information and room labels. To capture more detailed spatial properties, we introduce structure nodes that encode the size and shape of each room. Our approach follows the VS-Graph framework [27], with YOSO [28] as the detection front-end. The structure node incorporates elements such as walls, doors, windows, blinds, and curtains. After segmentation, we perform RANSAC [29] plane fitting on the point cloud data associated with each segmentation mask. We then fit a bounding box to all the inliers associated with that fitted plane. To ensure accurate wall mapping, we require that each wall be observed multiple times before being added to the graph. We further apply Euclidean clustering to the RANSAC output to prevent the generation of long, spurious walls, particularly when walls from different rooms align and RANSAC treats them as a single plane.

B. Reasoning and Information Gain Estimation

Let $x_k \in \text{SE}(2)$ denote the location of the robot at time k and Y_k denote the observation at time k , the realization of this random variable will be denoted by y_k . The goal of active perception [6] is to select a next viewpoint x_{k+1} that maximizes the mutual information between the next observation Y_{k+1} and past observations (y_1, \dots, y_k)

$$\begin{aligned} \text{I}(Y_{k+1}, y_{1:k} | x) &= \text{I}(Y_{k+1}, G_k | x) \\ &= \text{H}(Y_{k+1} | x) - \text{H}(Y_{k+1} | x, G_k). \end{aligned} \quad (1)$$

The first equality follows because the current scene graph denoted by G_k is a representation of the past observations.

selects the farthest waypoint along the global path in free space, and uses A* again to compute the shortest path in SE(2) to this waypoint. We observed that using this scene-graph planner works reasonably well. But a global occupancy grid is more reliable (although due to localization errors in the SDF, this global occupancy grid is also inaccurate at various places in the scene). For all experiments in this paper, we therefore use a global occupancy grid for high-level navigation and a local occupancy grid for low-level navigation.

IV. EXPERIMENTS

A. Setup

We conduct simulation experiments in large-scale indoor apartment scenes using the HM3D [30] dataset. HM3D is a large scale dataset with about 1000 different scenes and floor spaces. We select three representative scenes ranging from small to large (scene 1 id: 00853; scene 2 id: 00871; scene 3 id: 00573). Navigation is performed in the Habitat simulator [31] on a laptop with an 8-core AMD Ryzen 7735H CPU and NVIDIA 4060 GPU. To construct ground-truth scene graphs for evaluation, we manually navigate the agent through each environment, ensuring that every accessible region is visited and every object is detected.

We use Gemini-2.5-Pro model [32] as our reasoning engine. We build 2 scene graphs using the mapping pipeline to represent $p(G_k)$ in Eq. (2). Each scene graph is provided with a subset of observation from sensors. For each constructed graph, we sample $m = 4$ in Eq. (3) complete scene graphs using the LLM, yielding a total of 8 samples from the latent complete scene graph space G . For the information-gain calculation, we perturb each scene graph $N = 4$ times in Eq. (4), randomly sample 300 candidate viewpoints distributed uniformly throughout the entire scene and choose $\lambda = 1$ in Eq. (5).

We compare our method against two baselines: (i) frontier-based exploration [15], a geometric method that identifies unexplored frontiers on an occupancy grid without semantic awareness, and (ii) SSMI exploration [10] which incorporates semantic information into the occupancy grid. During exploration, SSMI evaluates potential geometric frontiers and ranks paths based on how much semantic uncertainty is reduced. For a fair comparison, we use the same motion planner as that of our method for the frontier-based baseline. For SSMI, we use their original planner because in their case, the planner is more intricately tied to their overall approach. For all methods, we perform a 2π yaw rotation at the end of each exploration step to maximize the visual information obtained at each location. All methods are evaluated under a shared path-length budget L_{\max} . Runs terminate when either (i) no geometric frontiers remain, or (ii) when the path length reaches L_{\max} . For the Frontier baseline, termination often occurs at a shorter overall exploration distance. Observe that the path length does not always reflect time spent in collecting observations (e.g., in-place yaw rotations). We therefore also analyze in terms of the time spent in collecting observations from the scene (excluding thereby, the time spent in actually computing the planned trajectory or querying the LLM).

B. Semantic grounding capability

This experiment evaluates how quickly and effectively an agent can build a semantic understanding of its environment. We assess the quality of the constructed scene graphs using two complementary metrics: F1 score and Graph Edit Distance (GED). The F1 score captures the accuracy of object detection by measuring the proportion of correctly identified objects.¹ In contrast, GED evaluates topological correctness, including rooms, objects, and their relationships. Formally, GED is the minimum sequence of node and edge edit operations required to transform graph G_1 into a graph isomorphic to G_2 .² Fig. 3 reports the F1 score and GED averaged across the three scenes as a function of the path length. The variance is smaller at the end because exploration of different scenes terminates at different distance. We also report F1 and GED at 10%, 50%, and 100% of a fixed exploration time budget in Table I. Frontier and our pipeline terminates at about the same time. For any fixed path length and time budget, our method has a higher F1 score and lower GED than baseline methods. This indicates faster and more topologically consistent semantic understanding.

C. Room finding capability

Beyond identifying semantically uncertain regions, a key strength of our framework lies in its ability to complete partially observed scenes. Since the latent complete scene graph is conditioned on the currently observed scene graph, different regions of the scene carry different levels of uncertainty. Hence, we can see that certain parts of the latent scene graph can be inferred with high confidence in the LLM prediction ensemble, while others remain ambiguous. To evaluate this capability, we design an experiment focused on discovering rooms that the robot has not directly observed. For this task, we define an *LLM-augmented graph* as the current scene graph, that contains all confident predictions. A prediction is considered confident if it is supported by a majority consensus, i.e., it appears in more than 50% of the ensemble outputs. Since the planner used in SSMI differs from ours, which may cause very different navigation behaviors, we restrict comparison here to the frontier-based pipeline.

Table II reports the results. Here, T_{pred} and D_{pred} denote the time and distance required for a successful prediction, while T_{find} and D_{find} denote the time and distance to actually discover the target room. Success requires satisfying two conditions: (i) the prediction must achieve majority agreement, and (ii) the Euclidean distance between the predicted and actual room locations must be within 2.5 meters. We also visualize the trajectories of our method versus the frontier-based approach in Fig. 4. As shown, our method consistently

¹If two objects have the same name and their center distance is within 0.5 m, we consider them a match. We restrict this calculation to object nodes, since structure and nothing nodes mainly serve to constrain the space of latent complete scene graph G .

²In our implementation, insertion and deletion of nodes and edges are assigned equal cost (1), ensuring balanced treatment of all graph components. Substitution is permitted only under specific conditions: room nodes must share the same name, while object nodes must share both the same name and the same parent, with spatial proximity within defined thresholds (0.5 m for objects and 4.0 m for rooms).

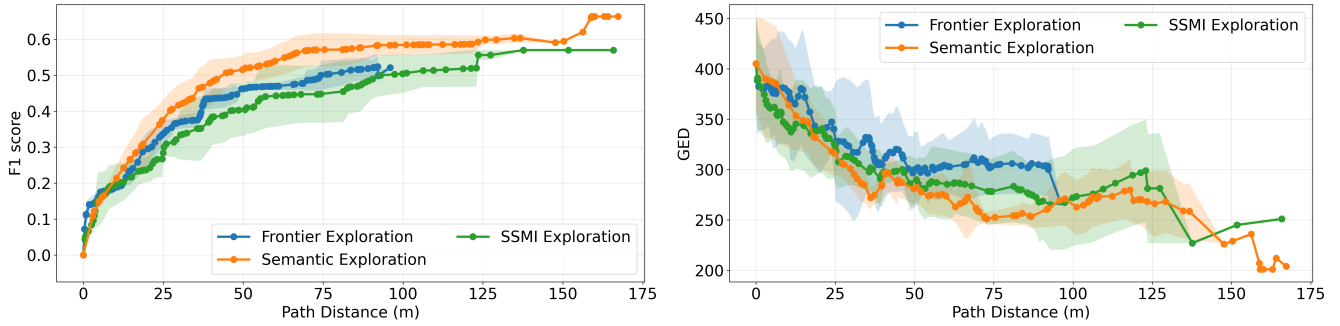


Fig. 3: Average F1 score and GED as a function of path length. The wider spacing of the dots along the curve for Semantic Exploration method indicates that our approach usually travels farther per step: the mean travel distance per step is 2 m for Frontier, 4.6 m for Semantic Exploration and 4 m for SSMI.

Method	00573						00853						00871					
	10%		50%		100%		10%		50%		100%		10%		50%		100%	
	F1↑	GED↓	F1↑	GED↓	F1↑	GED↓	F1↑	GED↓	F1↑	GED↓	F1↑	GED↓	F1↑	GED↓	F1↑	GED↓	F1↑	GED↓
Frontier	17.6	303.6	46.3	265.2	52.1	268.0	16.9	398.6	45.0	313.8	48.3	335.0	20.1	430.9	45.4	338.0	57.4	310.0
Semantic	17.3	306.3	53.6	237.7	66.3	204.0	25.1	368.3	58.6	245.1	59.0	294.0	33.0	375.2	61.5	262.7	61.5	286.0

TABLE I: F1 and GED at 10%, 50%, and 100% navigation time budgets across three scenes for two methods.

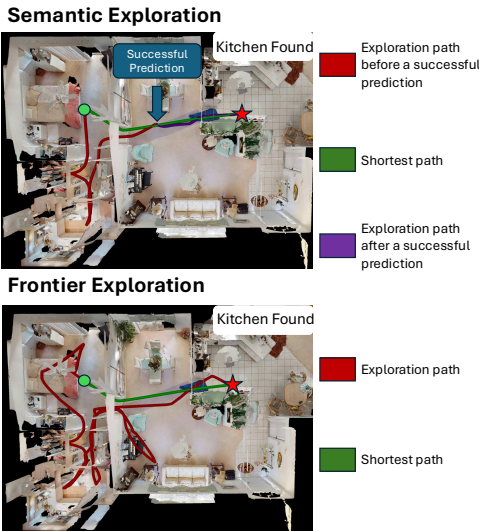


Fig. 4: Visualization of the paths taken to locate a kitchen: semantic exploration vs. baseline. Semantic exploration follows a shorter trajectory and successfully predicts the kitchen’s location before it is observed.

outperforms the baseline and it can reliably predict potential target rooms before they are directly observed. This is very interesting because in this experiment, we did not explicitly tell LLM what target we want to find in the prompt.

D. Ablation Study

We next provide a qualitative understanding of our system to prove the effectiveness of our scene graph design. We evaluate the contribution of each node type with an ablation on a single scene, while progressively enabling different types of constraints: (A) Baseline; (B) Baseline + *Nothing* (negative-space) nodes; (C) Baseline + *Nothing* + *Structure*

nodes; and (D) Baseline + *Nothing* + *Structure* + *Door* nodes. Fig. 5 overlays predicted boxes (red) on existing boxes (gray). Relative to (A), adding *Nothing* nodes in (B) reduces incorrect object placement (e.g., a TV stand) by explicitly encoding free space. Adding *Structure* nodes in (C) constrains completions to respect room boundaries and reduces proposals being outside the enclosed space or the window. Finally, adding *Door* nodes in (D) guides new-room proposals behind doors where a new room is most likely to be found.

E. Discussion

Exploration Behavior Our method has a large mean travel distance per exploration step. This is because it can “see farther” than frontier-based planners that only use geometric information. Our approach proposes semantically-informed waypoints that are far away from the current location of the robot (likely rooms/objects beyond the closest frontier) and de-prioritizes small gaps inside rooms which are guessed with relative certainty by the LLM. This explains the wider marker spacing in Fig. 3. Longer steps also reduce the time required for navigation (fewer turns). For a fixed path length, all methods perform roughly the same at the beginning. This is because incorporating a 360-degree scan after each step quickly and effectively gathers local information. Our results are better (higher F1, lower GED) at later stages because viewpoint selection is driven by expected semantic information gain. This avoids frontiers that lead to empty space or viewpoints with poor visibility. We also observe that our pipeline will sometimes revisit mapped areas to correct previous mistakes. These behaviors explain the higher accuracy of our method in the end.

In our experiments, we observe that SSMI sometimes favors farther geometric frontiers over closer ones. While this still drives exploration forward, it often results in circuitous trajectories. We attribute this behavior to how

Exploration Method	Environment	Target	T _{pred} (s) ↓	D _{pred} (m) ↓	T _{find} (s) ↓	D _{find} (m) ↓
Frontier	00853	Second Bedroom	N/A	N/A	258	38
Semantic	6 rooms 207.63m ²		158	34	168	36
Frontier	00871	Bathroom	N/A	N/A	86	11
Semantic	9 rooms 235.03m ²		23	3	37	6
Frontier	00871	Kitchen	N/A	N/A	261	37
Semantic	9 rooms 235.03m ²		65	13	105	18
Frontier	00573	Bathroom	N/A	N/A	48	5
Semantic	11 rooms 537.81m ²		19	3	37	5

TABLE II: Quantitative Results of Room-finding Experiments.

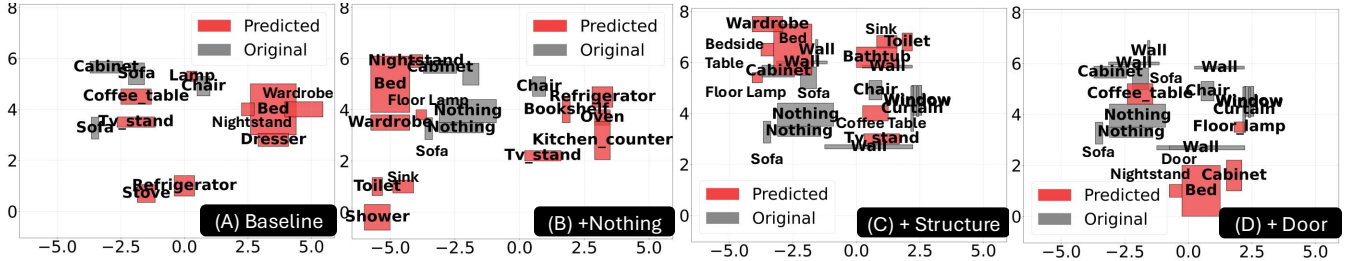


Fig. 5: Ablation on scene-graph node types. Constraints are enabled progressively: (A) Baseline; (B) +Nothing (free-space); (C) +Nothing+Structure; (D) +Nothing+Structure+Door.

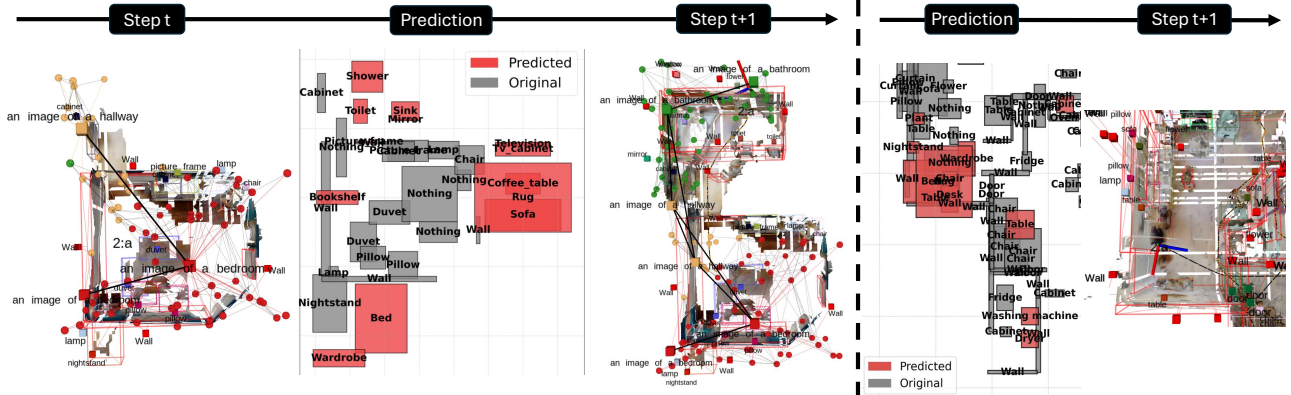


Fig. 6: **Left:** The LLM successfully predicts a bathroom above the bedroom for the robot to navigate to. **Right:** LLM incorrectly predicts a bedroom in the bottom-left corner, misleading the agent to navigate toward an already observed empty region.

semantics are stored at the voxel level. Because the object detector introduces noise, even objects that are generally well recognized may produce many voxels marked as uncertain. To reduce this noise-driven uncertainty in the semantic map, the metric prioritizes exploration steps that yields larger reductions in uncertainty, which are often associated with distant frontiers rather than nearby ones. Thus, although SSMI expands the explored space, it does so in a less efficient manner. By contrast, our scene-graph-based representation avoids voxel-level noise and allows reasoning directly at the object and room level, leading to shorter and more purposeful exploration paths.

Effect of scene layout Table I shows that in scene 00573 all the methods perform nearly the same at the 10% navigation time budget. This pattern is explained by the scene layout. The scene begins with a long corridor and five adjacent rooms, so new areas must be revealed sequentially. In that narrow corridor, a 360° spin after each step already gives the Frontier baseline close-to-optimal behavior. By contrast, scenes 00853 and 00871 contain large open areas. Our metric usually selects longer range viewpoints, which lets the robot see farther and cover space faster.

Prediction Behavior We find that hallways and doors serve as strong cues for the LLM to hypothesize additional rooms. The left part of Fig. 6 shows a successful case: at exploration step t , the robot has mapped a bedroom and a hallway; conditioned on these cues, the LLM predicts a bathroom near the hallway, a living room to the right, and a bedroom at the bottom. The next viewpoint selected by our information-gain objective lies at the top. At step $t+1$, the robot uncovers a bathroom at the predicted location, confirming that part of the hypothesis (the remaining proposals require further evidence). Doors can also mislead the LLM. The right part of Fig. 6 is an example of this. Although the left side had already been mapped and was simply empty living-room space, the LLM proposed a bedroom there near a door, prompting an uninformative revisit that yielded little new information.

V. LIMITATIONS AND FUTURE WORK

While our framework demonstrates the potential of semantic exploration, several limitations remain. First, the LLM we use is not trained specifically for scene expansion. As a result, its proposal distribution can diverge from the true scene distribution, particularly in larger and more complex

environments. We use about 8 samples of the completed scene graph to estimate the information gain, but this is not really sufficient to capture the diversity of plausible completions.

Second, the LLM occasionally hallucinates totally implausible viewpoints (e.g., placing a bathroom inside a bedroom). To work around this issue in experiments, we manually rejected some outputs of the LLM (about 0.08 rejections per meter averaged across the three scenes; with at most two rejections “allowed” per step). Our system simply provided the same query again to the LLM after such a rejection. Hallucination in LLMs remains a major problem, and such measures are necessary to develop LLM-based systems that can perform robustly. We aim to develop automated plausibility checks for rejecting these LLM outputs in the future.

Third, the reasoning time of our system is somewhat long. Our pipeline samples a total of 8 scene graphs from the LLM, and to improve results and reduce hallucination, we submit one more query for the LLM to refine its initial generation. On average, a single refinement takes about 70 seconds, and the full reasoning process in our pipeline requires roughly two and a half minutes even with multi-threaded execution. Throughout the paper, all reported times exclude LLM reasoning and include only navigation time.³

For future work, we aim to develop a dedicated reasoning model for scene understanding. We believe this will narrow the generalization gap and mitigate long reasoning time. Another promising direction is to extend our framework to handle a broader range of item categories, such as objects, exits, and people, thereby improving its applicability to more real-world exploration tasks.

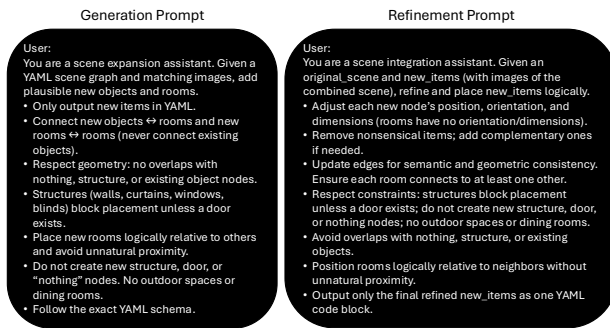


Fig. 7: A summarized version of the generation and refinement prompts used in all experiments.

REFERENCES

[1] S. He, “Mathematical theory and algorithms for scene semantics in robotics,” B.S. Thesis, University of Pennsylvania, 2025.

[2] J. Kirby, *An Invitation to Model Theory*, 2019.

[3] R. W. Floyd, “Assigning meanings to programs,” in *Program Verification: Fundamental Issues in Computer Science*, 1993, pp. 65–81.

[4] D. Maggio, Y. Chang, N. Hughes, M. Trang, D. Griffith, C. Dougherty, E. Cristofalo, L. Schmid, and L. Carlone, “Clio: Real-time task-driven open-set 3d scene graphs,” *IEEE RA-L*, 2024.

[5] R. Bajcsy, Y. Aloimonos, and J. K. Tsotsos, “Revisiting active perception,” *Autonomous Robots*, vol. 42, no. 2, pp. 177–196, 2018.

[6] H. Siming, C. D. Hsu, D. Ong, Y. S. Shao, and P. Chaudhari, “Active perception using neural radiance fields,” in *ACC*, 2024, pp. 4353–4358.

³Prompts have a large effect on LLM outputs. Therefore, we provide a concise summary of the prompts used across all experiments in Fig. 7.

[7] N. Hughes, Y. Chang, and L. Carlone, “Hydra: A real-time spatial perception system for 3D scene graph construction and optimization,” 2022.

[8] A. Hornung, K. M. Wurm, M. Bennewitz, C. Stachniss, and W. Burgard, “Octomap: An efficient probabilistic 3d mapping framework based on octrees,” *Autonomous robots*, vol. 34, no. 3, pp. 189–206, 2013.

[9] H. Oleynikova, Z. Taylor, M. Fehr, R. Siegwart, and J. Nieto, “Voxblox: Incremental 3d euclidean signed distance fields for on-board map planning,” in *IROS*, 2017, pp. 1366–1373.

[10] A. Asgharivaskasi and N. Atanasov, “Semantic octree mapping and Shannon mutual information computation for robot exploration,” *T-RO*, vol. 39, no. 3, pp. 1910–1928, 2023.

[11] B. Mildenhall, P. P. Srinivasan, M. Tancik, J. T. Barron, R. Ramamoorthi, and R. Ng, “Nerf: Representing scenes as neural radiance fields for view synthesis,” *CACM*, vol. 65, no. 1, pp. 99–106, 2021.

[12] B. Kerbl, G. Kopanas, T. Leimkühler, and G. Drettakis, “3d gaussian splatting for real-time radiance field rendering,” *ACM Trans. Graph.*, vol. 42, no. 4, pp. 139–1, 2023.

[13] S. Zhi, T. Laidlow, S. Leutenegger, and A. J. Davison, “In-place scene labelling and understanding with implicit scene representation,” in *ICCV*, 2021, pp. 15 838–15 847.

[14] M. Strong, B. Lei, A. Swann, W. Jiang, K. Daniilidis, and M. Kennedy, “Next best sense: Guiding vision and touch with fisherrf for 3d gaussian splatting,” in *ICRA*, 2025.

[15] B. Yamauchi, “A frontier-based approach for autonomous exploration,” in *CIRA*, 1997, pp. 146–151.

[16] Y. Tao, E. Iceland, B. Li, E. Zwecher, U. Heinemann, A. Cohen, A. Avni, O. Gal, A. Barel, and V. Kumar, “Learning to explore indoor environments using autonomous micro aerial vehicles,” in *ICRA*, 2024.

[17] A. Bircher, M. Kamel, K. Alexis, H. Oleynikova, and R. Siegwart, “Receding horizon” next-best-view” planner for 3d exploration,” in *ICRA*, 2016, pp. 1462–1468.

[18] B. Charrow, S. Liu, V. Kumar, and N. Michael, “Information-theoretic mapping using cauchy-schwarz quadratic mutual information,” in *ICRA*, 2015, pp. 4791–4798.

[19] S. He, Y. Tao, I. Spasojevic, V. Kumar, and P. Chaudhari, “An active perception game for robust information gathering,” in *ICRA*, 2025, pp. 14 168–14 174.

[20] W. Jiang, B. Lei, and K. Daniilidis, “Fisherrf: Active view selection and uncertainty quantification for radiance fields using fisher information,” in *ICCV*, 2024.

[21] D. S. Chaplot, D. P. Gandhi, A. Gupta, and R. R. Salakhutdinov, “Object goal navigation using goal-oriented semantic exploration,” *NeurIPS*, vol. 33, pp. 4247–4258, 2020.

[22] J. Chen, G. Li, S. Kumar, B. Ghanem, and F. Yu, “How to not train your dragon: Training-free embodied object goal navigation with semantic frontiers,” *RSS*, 2023.

[23] A. Wang, L. Liu, H. Chen, Z. Lin, J. Han, and G. Ding, “Yoloe: Real-time seeing anything,” *arXiv preprint arXiv:2503.07465*, 2025.

[24] X. Zhao, W. Ding, Y. An, Y. Du, T. Yu, M. Li, M. Tang, and J. Wang, “Fast segment anything,” *arXiv preprint arXiv:2306.12156*, 2023.

[25] A. Radford, J. W. Kim, C. Hallacy, A. Ramesh, G. Goh, S. Agarwal, G. Sastry, A. Askell, P. Mishkin, J. Clark, *et al.*, “Learning transferable visual models from natural language supervision,” in *ICML*, 2021, pp. 8748–8763.

[26] W. E. Lorensen and H. E. Cline, “Marching cubes: A high resolution 3d surface construction algorithm,” in *Seminal graphics*, 1998, pp. 347–353.

[27] A. Tourani, S. Ejaz, H. Bavle, D. Morilla-Cabello, J. L. Sanchez-Lopez, and H. Voos, “vs-graphs: Integrating visual slam and situational graphs through multi-level scene understanding,” *arXiv preprint arXiv:2503.01783*, 2025.

[28] J. Hu, L. Huang, T. Ren, S. Zhang, R. Ji, and L. Cao, “You only segment once: Towards real-time panoptic segmentation,” in *CVPR*, 2023, pp. 17 819–17 829.

[29] M. A. Fischler and R. C. Bolles, “Random sample consensus: a paradigm for model fitting with applications to image analysis and automated cartography,” *CACM*, vol. 24, no. 6, pp. 381–395, 1981.

[30] S. K. Ramakrishnan, A. Gokaslan, E. Wijmans, O. Maksymets, A. Clegg, J. M. Turner, E. Undersander, W. Galuba, A. Westbury, A. X. Chang, M. Savva, Y. Zhao, and D. Batra, “Habitat-matterport 3d dataset (HM3d): 1000 large-scale 3d environments for embodied AI,” in *NeurIPS Datasets and Benchmarks Track*, 2021.

[31] M. Savva, A. Kadian, O. Maksymets, Y. Zhao, E. Wijmans, B. Jain, J. Straub, J. Liu, V. Koltun, J. Malik, *et al.*, “Habitat: A platform for embodied ai research,” in *ICCV*, 2019, pp. 9339–9347.

[32] G. Comanici, E. Bieber, M. Schaekermann, I. Pasupat, N. Sachdeva,

I. Dhillon, M. Blistein, O. Ram, D. Zhang, E. Rosen, *et al.*, “Gemini 2.5: Pushing the frontier with advanced reasoning, multimodality, long context, and next generation agentic capabilities,” *arXiv preprint arXiv:2507.06261*, 2025.